Title

Metabolic imaging detects elevated glucose flux through the pentose phosphate pathway associated with TERT expression in low-grade gliomas

Journal

Neuro-Oncology, 23(9)

ISSN

1522-8517

Authors

Viswanath, Pavithra

Batsios, Georgios

Ayyappan, Vinay

et al.

Publication Date

2021-09-01

DOI

10.1093/neuonc/noab093

Peer reviewed

Neuro-Oncology
23(9), 1509–1522, 2021 | doi:10.1093/neuonc/noab093 | Advance Access date 17 April 2021

Metabolic imaging detects elevated glucose flux through the pentose phosphate pathway associated with TERT expression in low-grade gliomas

Pavithra Viswanath, Georgios Batsios, Vinay Ayyappan, Céline Taglang, Anne Marie Gillespie, Peder E. Z. Larson, H. Artee Luchman, Joseph F. Costello, Russell O. Pieper, and Sabrina M. Ronen

Department of Radiology and Biomedical Imaging, University of California San Francisco, San Francisco, California, USA (P.V., G.B., V.A., C.T., A.M.G., P.E.Z.L., S.M.R.); Department of Cell Biology and Anatomy and Hotchkiss Brain Institute, University of Calgary, Calgary, Alberta, Canada (H.A.L.); Department of Neurological Surgery, University of California San Francisco, San Francisco, California, USA (J.F.C., R.O.P.)

Corresponding Author: Pavithra Viswanath, PhD, Department of Radiology and Biomedical Imaging, University of California San Francisco, 1700 4th St, San Francisco, CA 94143, USA (Pavithra.Viswanath@ucsf.edu).

Abstract

Background. Telomerase reverse transcriptase (TERT) is essential for tumor proliferation, including in low-grade oligodendrogliomas (LGOGs). Since TERT is silenced in normal cells, it is also a therapeutic target. Therefore, noninvasive methods of imaging TERT are needed. Here, we examined the link between TERT expression and metabolism in LGOGs, with the goal of leveraging this information for noninvasive magnetic resonance spectroscopy (MRS)-based metabolic imaging of LGOGs.

Methods. Immortalized normal human astrocytes with doxycycline-inducible TERT silencing, patient-derived LGOG cells, orthotopic tumors, and LGOG patient biopsies were studied to determine the mechanistic link between TERT expression and glucose metabolism. The ability of hyperpolarized [U-^{13}C, U-^{2}H]-glucose to noninvasively assess TERT expression was tested in live cells and orthotopic tumors.

Results. TERT expression was associated with elevated glucose flux through the pentose phosphate pathway (PPP), elevated NADPH, which is a major product of the PPP, and elevated glutathione, which is maintained in a reduced state by NADPH. Importantly, hyperpolarized [U-^{13}C, U-^{2}H]-glucose metabolism via the PPP noninvasively reported on TERT expression and response to TERT inhibition in patient-derived LGOG cells and orthotopic tumors. Mechanistically, TERT acted via the sirtuin SIRT2 to upregulate the glucose transporter GLUT1 and the rate-limiting PPP enzyme glucose-6-phosphate dehydrogenase.

Conclusions. We have, for the first time, leveraged a mechanistic understanding of TERT-associated metabolic reprogramming for noninvasive imaging of LGOGs using hyperpolarized [U-^{13}C, U-^{2}H]-glucose. Our findings provide a novel way of imaging a hallmark of tumor immortality and have the potential to improve diagnosis and treatment response assessment for LGOG patients.

Key Points

- TERT expression mechanistically reprograms glucose metabolism via the pentose phosphate pathway.
- TERT-linked metabolic reprogramming can be leveraged for noninvasive glioma imaging using hyperpolarized ^{13}C-glucose.

Importance of the Study

MRI is the mainstay of glioma imaging. However, MRI fails to distinguish true tumor from morphologically similar areas of gliosis, edema, and necrosis. MRI also does not distinguish tumor recurrence from treatment-induced effects such as pseudoprogression and pseudoresponse. Therefore, there is a need to identify noninvasive methods that track molecular hallmarks of tumor proliferation. Telomere maintenance is one such hallmark and most cancers, including LGOGs, maintain telomere length via TERT expression. Here, we show that TERT acts via the sirtuin SIRT2 to reprogram glucose metabolism through the PPP, resulting in elevated levels of the redox metabolites NADPH and glutathione in LGOGs. Importantly, we have leveraged this information for noninvasive hyperpolarized [U-^{13}C, U-^{2}H]-glucose-based imaging of TERT expression in patient-derived LGOG models *in vivo*. Our study enables noninvasive visualization of a hallmark of tumor proliferation and has the potential to improve longitudinal analysis of tumor burden and treatment response in LGOG patients.

Telomere maintenance is a fundamental hallmark of cancer.[1] Telomeres are specialized cap-like nucleoprotein structures that protect chromosomal ends from DNA damage.[2] Progressive telomere shortening during cell division leads to growth arrest and constitutes a barrier to uncontrolled proliferation.[1,2] Tumor cells, therefore, need a mechanism of maintaining telomere length. Most tumors maintain telomere length by reactivating the expression of telomerase reverse transcriptase (TERT), which is the catalytic component of the enzyme telomerase that synthesizes telomeric DNA.[2,3] TERT expression is silenced at birth in normal somatic cells, with the exception of stem cells, and is reactivated in tumor cells via TERT promoter mutations.[3–5] Importantly, TERT promoter mutations are a prerequisite for rapid glioma growth *in vivo*,[6] further underscoring the crucial role of TERT in glioma proliferation.

The clinical relevance of TERT arises from its diagnostic, prognostic, and therapeutic potential. Among low-grade gliomas defined by mutations in isocitrate dehydrogenase (IDHmut),[7] TERT promoter mutations occur frequently in low-grade oligodendrogliomas (LGOGs) but rarely in low-grade astrocytomas,[7,8] which use a TERT-independent telomere maintenance mechanism known as the alternative lengthening of telomeres (ALT) pathway.[9,10] As a result, assessment of TERT status is a valuable addition to glioma classification.[11] Research also suggests that clinically meaningful patient prognosis can be achieved on the basis of three molecular markers, ie, IDHmut, 1p19q co-deletion, and TERT promoter mutations.[8] TERT is also an attractive therapeutic target since TERT expression is silenced in normal cells or expressed in a tightly regulated manner from the wild-type TERT promoter in stem cells.[2,3] Since TERT promoter mutations are specific to tumor cells,[3] disrupting TERT expression from the mutant TERT promoter has therapeutic potential.[5]

Previous studies have linked TERT expression to metabolic reprogramming in cancer.[12] TERT inhibition in melanoma cells downregulates glucose transport and glycolysis.[13] In primary glioblastoma cells, pharmacological or genetic inhibition of TERT abrogates glucose flux through the pentose phosphate pathway (PPP)[14] and represses fatty acid synthesis.[15] TERT has also been linked to altered cellular redox via modulation of reduced glutathione (GSH).[16,17]

Magnetic resonance spectroscopy (MRS) is a safe, nonradioactive, noninvasive method of imaging metabolism.[18] Thermally polarized ^{13}C-MRS following administration of ^{13}C-labeled precursors traces metabolic fluxes, but its inherently low sensitivity limits its translational value.[19] However, hyperpolarization enhances the signal-to-noise ratio (SNR) of ^{13}C-MRS by >10000-fold and provides a noninvasive method of imaging metabolic fluxes.[18] Importantly, hyperpolarized ^{13}C-MRS is a translational method that is in clinical trials,[18] and its feasibility has been established in glioma patients.[19,20]

Due to its inherent link to tumor proliferation, TERT has the potential to serve as a biomarker of tumor burden and response to therapy. The objective of this study was to examine the link between TERT expression and glucose metabolism in LGOGs with the ultimate goal of leveraging this information for noninvasive MRS-based metabolic imaging. Using genetically engineered and patient-derived LGOG models, we show that TERT expression is mechanistically associated with elevated PPP flux and higher antioxidant capacity. Importantly, we show that hyperpolarized [U-^{13}C, U-^{2}H]-glucose noninvasively reports on TERT expression in LGOG models *in vivo*.

Materials and Methods

Detailed experimental procedures are provided in the Supplementary material.

Cell Culture

Immortalized IDHmut-expressing p53/pRb-deficient normal human astrocytes ($NHA_{CONTROL}$) have been previously described.[21] The doxycycline-inducible NHA_{TERT+} model was generated by engineering $NHA_{CONTROL}$ cells such that TERT expression was regulated from a tetracycline (TET)-off promoter and could be silenced upon doxycycline addition (0.4 μg/mL). RNA interference was carried out using two non-overlapping siRNA pools (Dharmacon). Human SIRT2 (Addgene) was overexpressed in $NHA_{TERT–}$ cells by transient transfection with polyethyleneimine.

NHAs that lack TERT and use the ALT pathway (NHA_{ALT}) have been previously described.[22] The ALT status of NHA_{ALT} cells was confirmed by measuring c-circles using telomeric qPCR with and without amplification by φ29 polymerase as described.[9,23] BT54 neurospheres and SF10417 cells were derived from LGOG patients and are grown in serum-free media.[24–27] Cell lines were routinely tested for mycoplasma contamination, authenticated by short tandem repeat fingerprinting, and assayed within 6 months.

Patient Biopsies

Biopsies from LGOG or astrocytoma patients or gliosis biopsies from epileptic patients were obtained from the UCSF Brain Tumor Center Biorepository in compliance with the informed consent policy.

Gene Expression and Activity

Steady-state metabolite levels (NADPH, NADP+, GSH, oxidized glutathione [GSSG], 6-phosphogluconate, lactate, reactive oxygen species [ROS]) and enzyme activities (telomerase, glucose-6-phosphate dehydrogenase [G6PDH], phosphoglycerate kinase 1 [PGK1], hexokinase) were determined using commercial kits. γH2AX and GLUT1 protein levels were measured by ELISA. Gene expression was assessed by quantitative RT-PCR and normalized to β-actin (Supplementary Methods).

^{13}C-MRS of Cell Extracts

Cells were cultured in a medium containing 5 mM [2-^{13}C]-glucose for 48 hours and metabolites extracted by the methanol-chloroform method.[26,27] ^{13}C-MR (30° flip angle, 3 second relaxation delay) spectra were obtained using a 11.7T spectrometer and peak integrals quantified to obtain metabolite concentrations. PPP flux was measured by quantifying the isotopomers of glutamate generated after PPP and glycolytic metabolism of [2-^{13}C]-glucose.[6] Glucose levels in media samples were quantified and uptake calculated as the difference in normalized fmol (Δfmol/cell) between 0 and 24 hours.

Hyperpolarized ^{13}C-MRS of Live Cells

Hyperpolarized [U-^{13}C, U-^{2}H]-glucose prepared as described[28] was dissolved in isotonic buffer (50 mM Tris-HCl, 13.3 mM $MgCl_2$ in D_2O, pH 8) and added to live cells[23] at a concentration of 12 mM. ^{13}C spectra were acquired on a 14T Bruker spectrometer (13° flip angle every 3 seconds for 300 seconds), and the area under the curve (AUC) for product was normalized to AUC of substrate and to cell number.

MRI

Animal studies were conducted in accordance with UCSF Institutional Animal Care and Use Committee guidelines. Doxycycline-inducible NHA_{TERT+}, NHA_{ALT}, or SF10417 cells (3×10^5 cells/10 μL) were intracranially injected into athymic nude rats (male, rnu/rnu homozygous).[23,26,27] T2-weighted MRI was performed on a 3T Bruker scanner using a spin-echo TurboRARE sequence (TE/TR = 64/3484 ms, FOV = 43 × 43 mm,^{2} 256 × 256, slice thickness = 1 mm, NA = 6).[23] Tumor volume was determined using in-house MATLAB codes (https://github.com/ViswanathLab/EPSI).[23] For doxycycline-mediated TERT silencing *in vivo*, doxycycline was administered in the feed *ad libitum* once tumors reached a volume of ~50 mm^3 as previously described.[29]

Hyperpolarized ^{13}C-MRS *in vivo*

Studies were performed on a Bruker 3T spectrometer. Following tumor implantation, tumor volume was monitored longitudinally by MRI and ^{13}C studies were performed once tumors reached a volume of ~50 mm.^{3} For slab studies, dynamic ^{13}C spectra were acquired from a 12 mm axial slab through the brain every 3 seconds using a flyback spectral-spatial radiofrequency pulse[30] following the intravenous injection of 150 mM hyperpolarized glucose. For imaging, a 2D flyback spectral-spatial echo-planar spectroscopic imaging (EPSI) pulse[30] was used with a final hyperpolarized glucose concentration of 250 mM. ^{13}C slab spectra were analyzed using Mnova. 2D EPSI data were analyzed using in-house MATLAB codes (https://github.com/ViswanathLab/EPSI).[23]

Statistical Analysis

All experiments were performed on a minimum of 3 samples ($n \geq 3$) and results presented as mean ± standard deviation. Statistical significance was assessed using an unpaired Student's *t* test or ordinary 1-way ANOVA with $P < .05$ considered significant. $^*P < .05$, $^{**}P < .01$, $^{***}P < .005$, $^{****}P < .0001$, ns = non-significant.

Results

TERT Expression Is Associated With Higher Glucose Flux via the PPP in LGOGs

To begin with, we studied genetically engineered immortalized normal human astrocytes (NHAs) that express IDHmut, which is characteristic of low-grade gliomas[7] and examined NHAs that lacked TERT ($NHA_{CONTROL}$) and those in which TERT expression was placed under the control of a doxycycline-inducible promoter. TERT expression and telomerase activity were observed in these cells in the absence of doxycycline (NHA_{TERT+}), significantly reduced upon doxycycline addition (NHA_{TERT-}) and restored following doxycycline removal ($NHA_{TERT+\ rescue}$; Supplementary Figure S1A, B). As additional controls, we also examined NHAs that do not express TERT, but instead use the ALT pathway (NHA_{ALT}) for telomere maintenance.[22,23] The ALT phenotype of NHA_{ALT} cells has previously been verified via quantification of c-circles, which are extrachromosomal DNA circles characteristic of the ALT pathway[22,23] (Supplementary Figure S1C).

Thermally polarized ^{13}C-MRS following administration of [2-^{13}C]-glucose can inform on flux via the PPP, which produces [4-^{13}C]-glutamate, and via glycolysis which yields [5-^{13}C]-glutamate (Figure 1A).[31] PPP flux was significantly higher in NHA_{TERT+} cells relative to $NHA_{CONTROL}$ and NHA_{ALT} (Figure 1B). Importantly, doxycycline-induced TERT silencing reduced PPP flux in NHA_{TERT-} cells to levels observed in $NHA_{CONTROL}$ and NHA_{ALT}, an effect that was reversed in $NHA_{TERT+\ rescue}$ cells. In order to confirm the clinical relevance of these results, we examined PPP flux in the patient-derived BT54 and SF10417 models.[25–27] We confirmed elevated TERT expression and telomerase activity in BT54 and SF10417 cells relative to $NHA_{CONTROL}$ (Supplementary Figure S1D, E). Silencing TERT in BT54 and SF10417 cells (Supplementary Figure S1F–I) significantly reduced PPP flux (Figure 1C and Supplementary Figure S1J), pointing to a causal link between TERT expression and PPP flux in LGOGs.

TERT Expression Is Associated With Higher Antioxidant Capacity in LGOGs

Glucose flux through the PPP is the largest NADPH-producing pathway.[32] NADPH, in turn, is essential for maintaining GSH in the reduced state[32] (see schematic in Figure 1D). Since our results linked TERT to higher PPP flux, we examined whether there was a concomitant change in NADPH and GSH. In line with PPP flux, NADPH and GSH were elevated in NHA_{TERT+} cells relative to $NHA_{CONTROL}$ and NHA_{ALT} (Figure 1E, F). Doxycycline-induced TERT silencing reduced NADPH and GSH, an effect that was rescued by doxycycline removal (Figure 1E, F). Importantly, TERT silencing significantly reduced NADPH and GSH in the BT54 (Figure 1G, H) and SF10417 (Supplementary Figure S2A, B) models. There was no change in NADP+ or GSSG in our models (Supplementary Figure S2C–H).

NADPH and GSH mitigate oxidative stress via suppression of ROS (see Figure 1D). TERT silencing significantly increased ROS in BT54 and SF10417 cells (Figure 1I, J). Conversely, TERT expression was associated with reduced ROS in the NHA_{TERT+} model (Supplementary Figure S2I). Taken together, these results link TERT expression to higher redox capacity and reduced oxidative stress in LGOGs.

Hyperpolarized [U-^{13}C, U-^{2}H]-Glucose Noninvasively Monitors TERT Expression in LGOG Cells

Hyperpolarized [U-^{13}C, U-^{2}H]-glucose has been used to probe glucose metabolism via glycolysis and the PPP in tumor cells other than gliomas.[28,33–36] Since our results linked TERT to higher PPP flux, we examined hyperpolarized [U-^{13}C, U-^{2}H]-glucose (T1 = 14 ± 2 seconds, 24% polarization, consistent with prior publications[28,33–36]) metabolism in our models. As shown in Figure 2A, we observed buildup of the PPP metabolite [1-^{13}C]-6-phosphogluconate (6-PG, 179.4 ppm; see schematic in Figure 1D) in NHA_{TERT+} cells. We did not observe [1-^{13}C]-lactate (183.4 ppm). Importantly, doxycycline-induced TERT silencing significantly reduced 6-PG production, and restoration of TERT expression via doxycycline removal restored 6-PG production (Figure 2B). The chemical shift of [1-^{13}C]-6-PG (179.4 ppm) is indistinguishable from that of [1-^{13}C]-3-phosphoglycerate (179.5 ppm) which can also be produced from glucose via glycolysis (see Figure 1D). Previous studies have disagreed on the assignment of this resonance and have variously assigned it to either 6-PG[28,33,35] or 3-phosphoglycerate.[34,36] In order to determine whether the resonance observed at 179.4 ppm in our experiments corresponded to 6-PG, we examined hyperpolarized [U-^{13}C, U-^{2}H]-glucose metabolism in NHA_{TERT+} cells in which expression of G6PDH, the enzyme responsible for 6-PG synthesis (see Figure 1D), was silenced (Supplementary Figure S3A, B). As shown in Figure 2C, D, the resonance at 179.4 ppm was lost in NHA_{TERT+} G6PDH– cells. In contrast, the 179.4 ppm peak was observed in NHA_{TERT+} cells in which PGK1, the glycolytic enzyme catalyzing 3-phosphoglycerate synthesis (see Figure 1D), was silenced (Supplementary Figure S3C, D), suggesting that 179.4 ppm peak likely corresponds to 6-PG.

In contrast to NHA_{TERT+} cells, NHA_{ALT} cells produced the glycolytic metabolite lactate (183.4 ppm, Figure 2E), but not 6-PG, from hyperpolarized [U-^{13}C, U-^{2}H]-glucose. In order to further confirm these results, we quantified 6-PG and lactate by spectrophotometric assays in extracts from cell suspensions that were rapidly frozen at the end of our hyperpolarized ^{13}C-MRS experiments. We detected 6-PG but not lactate in NHA_{TERT+} extracts and lactate but not 6-PG in NHA_{ALT} extracts (Supplementary Figure S3E). NHA_{TERT-} extracts showed significantly reduced 6-PG relative to NHA_{TERT+}, but lactate could not be detected. Silencing G6PDH, but not PGK1, in NHA_{TERT+} cells reduced 6-PG production (Supplementary Figure S3F). We did not observe lactate in extracts from NHA_{TERT+} G6PDH– or PGK– cells (Supplementary Figure S3G). These results suggest that, within the temporal window of the hyperpolarized ^{13}C-MRS experiment (~5 minutes), hyperpolarized [U-^{13}C, U-^{2}H]-glucose metabolism to 6-PG distinguishes TERT-expressing cells from cells lacking TERT.

We confirmed the clinical relevance of these results in the patient-derived BT54 and SF10417 models. TERT silencing abrogated 6-PG production from hyperpolarized [U-^{13}C, U-^{2}H]-glucose in both models (Figure 2F, G and Supplementary Figure S3H, I). To assess whether hyperpolarized [U-^{13}C, U-^{2}H]-glucose provides a readout of response to TERT inhibition, we examined SF10417 cells treated with the telomerase inhibitor 6-thio-2′-deoxyguanosine.[37] Induction of DNA damage (Supplementary Figure S3J) was associated with significantly reduced 6-PG production from hyperpolarized [U-^{13}C, U-^{2}H]-glucose in 6-thio-2′-deoxyguanosine-treated SF10417 cells (Figure 2H). Collectively, these results suggest that hyperpolarized [U-^{13}C, U-^{2}H]-glucose flux to 6-PG reports on TERT expression and response to telomerase inhibition in LGOG cells.

Hyperpolarized [U-^{13}C, U-^{2}H]-Glucose Metabolism to 6-PG Noninvasively Monitors TERT Expression in LGOGs *In Vivo*

Next, we examined the feasibility of imaging TERT *in vivo* using hyperpolarized [U-^{13}C, U-^{2}H]-glucose. Dynamic ^{13}C spectra were acquired from a 12 mm slab of the brain following intravenous injection of hyperpolarized [U-^{13}C,

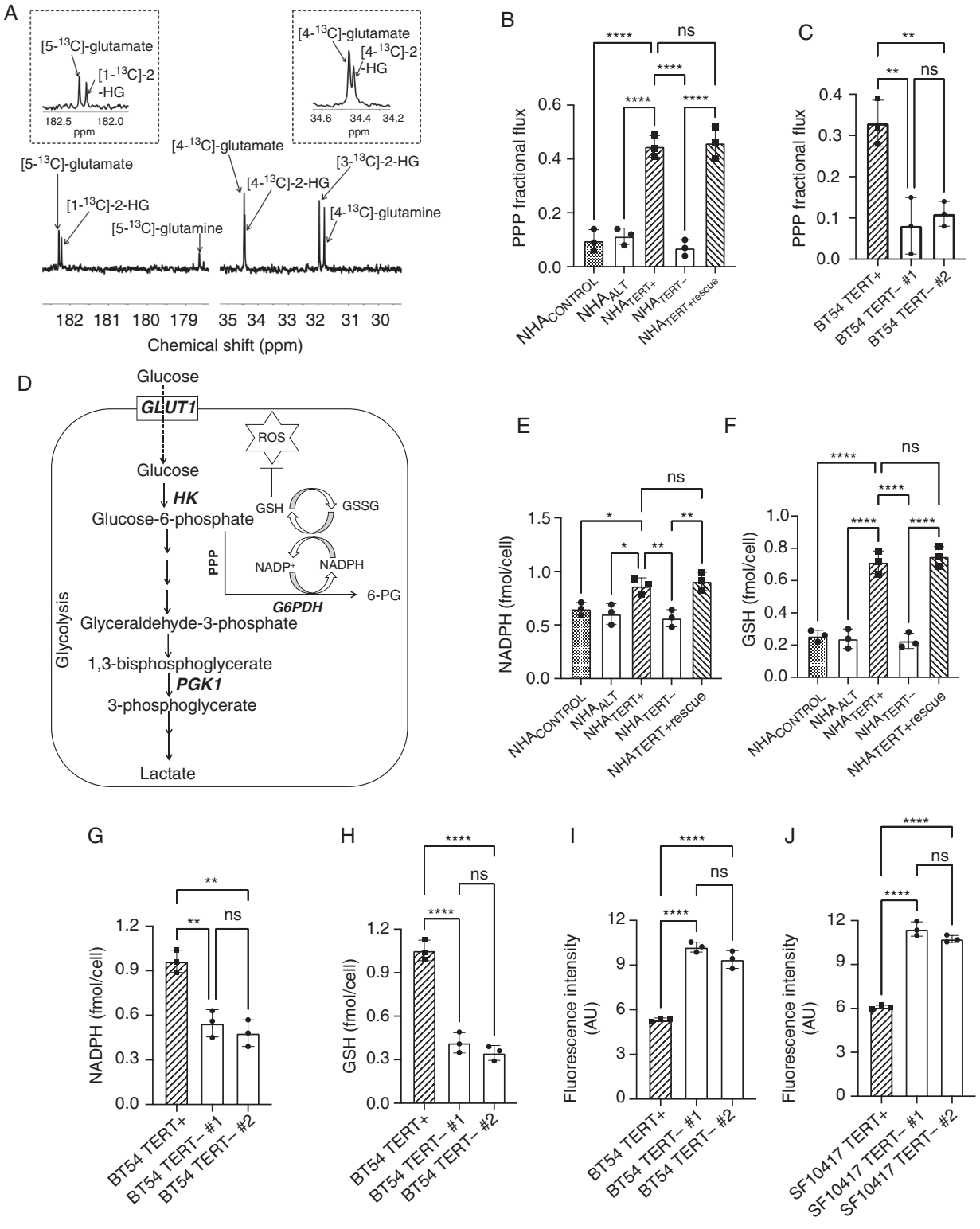

Fig. 1 TERT expression is associated with elevated PPP flux in LGOG cells. (A) Representative ^{13}C-MR spectrum from NHA_{TERT+} cells incubated with [2-^{13}C]-glucose. Peaks for glutamate, glutamine, and 2-hydroxyglutarate (2-HG; product of the IDHmut enzyme[26,27]) are labeled. Insets show an expansion of the regions corresponding to [5-^{13}C]-glutamate (left) and [4-^{13}C]-glutamate (right). (B) PPP flux in $NHA_{CONTROL}$, NHA_{ALT}, NHA_{TERT+}, NHA_{TERT-}, and $NHA_{TERT+\ rescue}$ cells. (C) Effect of TERT silencing on PPP flux in BT54 neurospheres. (D) Schematic illustration of glucose metabolism via the PPP and glycolysis. NADPH (E) and GSH (F) in $NHA_{CONTROL}$, NHA_{ALT}, NHA_{TERT+}, NHA_{TERT-}, and $NHA_{TERT+\ rescue}$ cells. Effect of TERT silencing on NADPH (G), GSH (H), and ROS (I) in BT54 neurospheres. Effect of TERT silencing on ROS (J) in SF10417 cells. Abbreviations: GSH, glutathione; LGOG, low-grade oligodendrogliomas; PPP, pentose phosphate pathway; ROS, reactive oxygen species; TERT, telomerase reverse transcriptase.

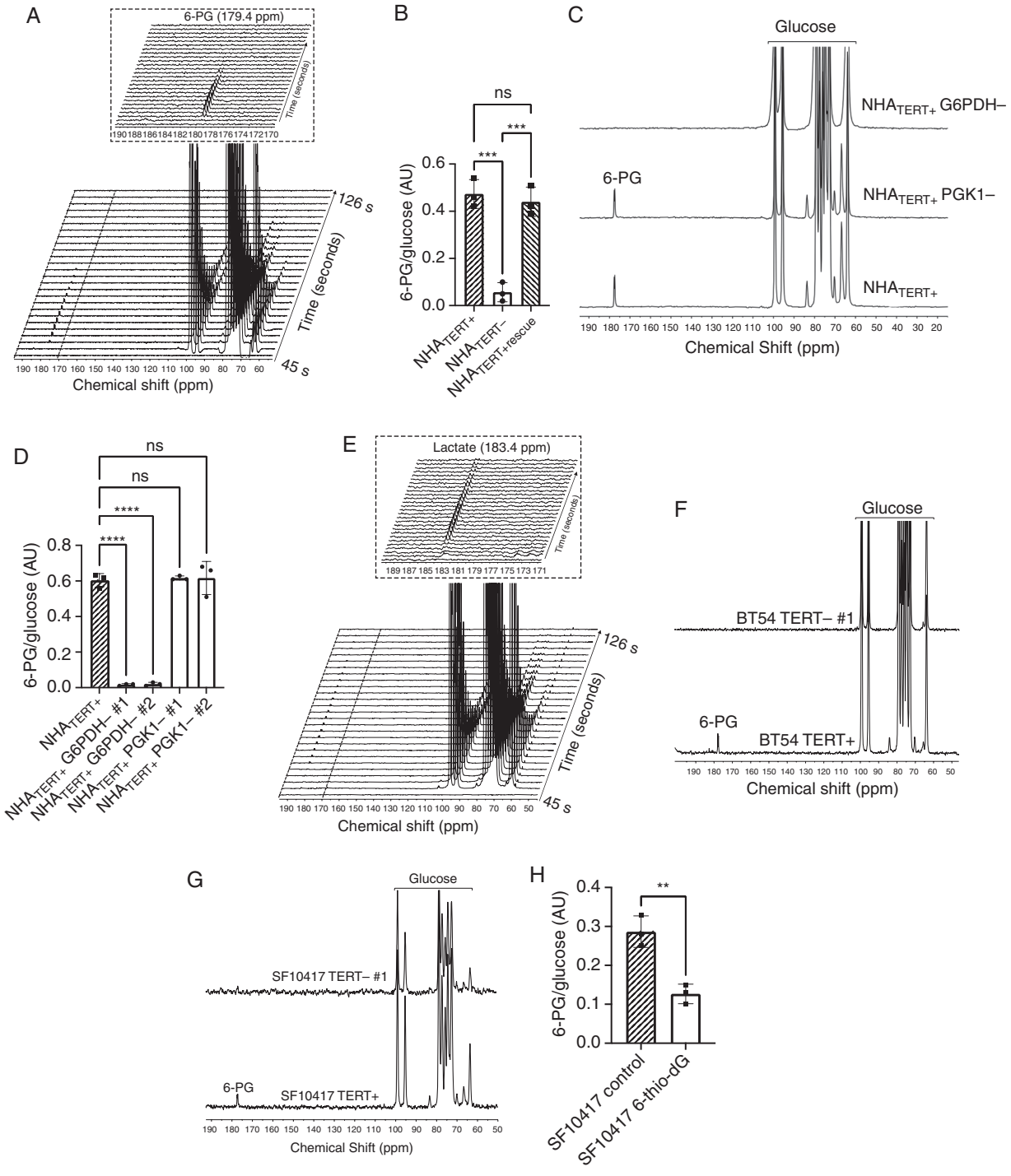

Fig. 2 TERT-linked increase in PPP flux can be noninvasively monitored using hyperpolarized [U-^{13}C, U-^{2}H]-glucose in live LGOG cells. (A) Representative spectral array of hyperpolarized [U-^{13}C, U-^{2}H]-glucose metabolism to 6-PG in NHA_{TERT+} cells. Inset shows an expansion of the region around 6-PG. (B) 6-PG/glucose ratio in the doxycycline-inducible NHA_{TERT+} model. Representative summed ^{13}C-MR spectra (C) and quantification of 6-PG production from hyperpolarized [U-^{13}C, U-^{2}H]-glucose (D) in NHA_{TERT+} cells in which G6PDH or PGK1 has been silenced. (E) Representative spectral array of hyperpolarized [U-^{13}C, U-^{2}H]-glucose metabolism to lactate in NHA_{ALT} cells. Inset shows an expansion of the region around lactate. Representative summed ^{13}C spectra showing the effect of TERT silencing on hyperpolarized [U-^{13}C, U-^{2}H]-glucose metabolism in the BT54 (F) or SF10417 (G) models. (H) Effect of 6-thio-2′-deoxyguanosine (6-thio-dG) on the 6-PG/glucose ratio in SF10417 cells. Abbreviations: LGOG, low-grade oligodendrogliomas; PPP, pentose phosphate pathway; TERT, telomerase reverse transcriptase.

U-^{2}H]-glucose into rats bearing orthotopic NHA_{TERT+}, SF10417, or NHA_{ALT} tumors (tumor volume ~50 mm^3). Consistent with our cell studies, we observed buildup of [1-^{13}C]-6-PG in NHA_{TERT+} and SF10417 tumor-bearing animals (Figure 3A, B), while NHA_{ALT} tumor-bearing rats produced [1-^{13}C]-lactate (Supplementary Figure S4A). Tumor-free controls produced neither 6-PG nor lactate (Supplementary Figure S4B). These differences are highlighted in the summed ^{13}C spectra shown in Figure 3C. The 6-PG/glucose ratio differentiated NHA_{TERT+} or SF10417 tumors from healthy brain (Figure 3D) while the lactate/glucose ratio differentiated NHA_{ALT} tumors from healthy brain (Supplementary Figure S4C). The temporal maximum (9 seconds post-injection; Figure 3E, F and Supplementary Figure S4D, E) and the SNR (Supplementary Figure S4F) of hyperpolarized [U-^{13}C, U-^{2}H]-glucose were similar in NHA_{TERT+}, SF10417, or NHA_{ALT} tumor-bearing animals and tumor-free controls, indicating that the observed differences in metabolism did not result from differences in glucose delivery. The maxima for 6-PG (15 seconds post-injection; Figure 3E, F) in TERT-expressing tumors and for lactate (21 seconds post-injection; Supplementary Figure S4D) in NHA_{ALT} tumors were delayed relative to glucose. Taken together with the lack of 6-PG or lactate in tumor-free rats, these results suggest that 6-PG or lactate production in tumor-bearing animals originates from metabolism within the tumor.

To assess the ability of hyperpolarized [U-^{13}C, U-^{2}H]-glucose to report on response to TERT inhibition *in vivo*,

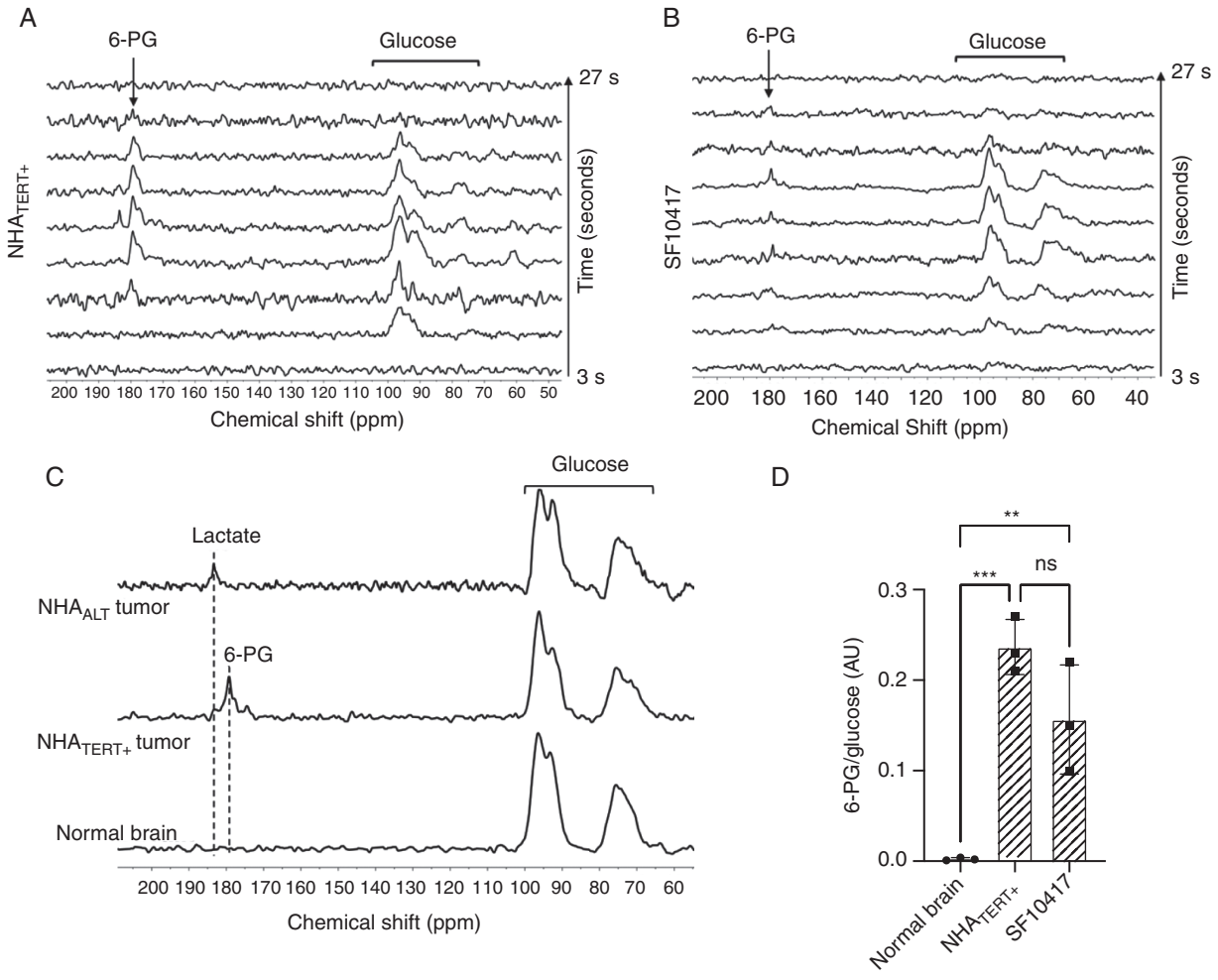

Fig. 3 Hyperpolarized [U-^{13}C, U-^{2}H]-glucose metabolism can be noninvasively monitored *in vivo*. Representative ^{13}C spectral array of hyperpolarized [U-^{13}C, U-^{2}H]-glucose metabolism in a rat bearing an orthotopic NHA_{TERT+} (A) or SF10417 (B) tumor. (C) Representative summed ^{13}C spectra of hyperpolarized [U-^{13}C, U-^{2}H]-glucose metabolism in rats bearing orthotopic NHA_{TERT+} or NHA_{ALT} tumors or tumor-free rats. (D) 6-PG/glucose ratio from slab studies in tumor-free normal brain, NHA_{TERT+} or SF10417 tumors. Dynamics of hyperpolarized [U-^{13}C, U-^{2}H]-glucose metabolism in rats bearing orthotopic NHA_{TERT+} (E) or SF10417 (F) tumors. Representative summed ^{13}C spectra (G) and quantification of 6-PG production from hyperpolarized [U-^{13}C, U-^{2}H]-glucose (H) in rats bearing orthotopic NHA_{TERT+} tumors before (NHA_{TERT+}) or after doxycycline-mediated TERT silencing (NHA_{TERT-}). Abbreviation: TERT, telomerase reverse transcriptase.

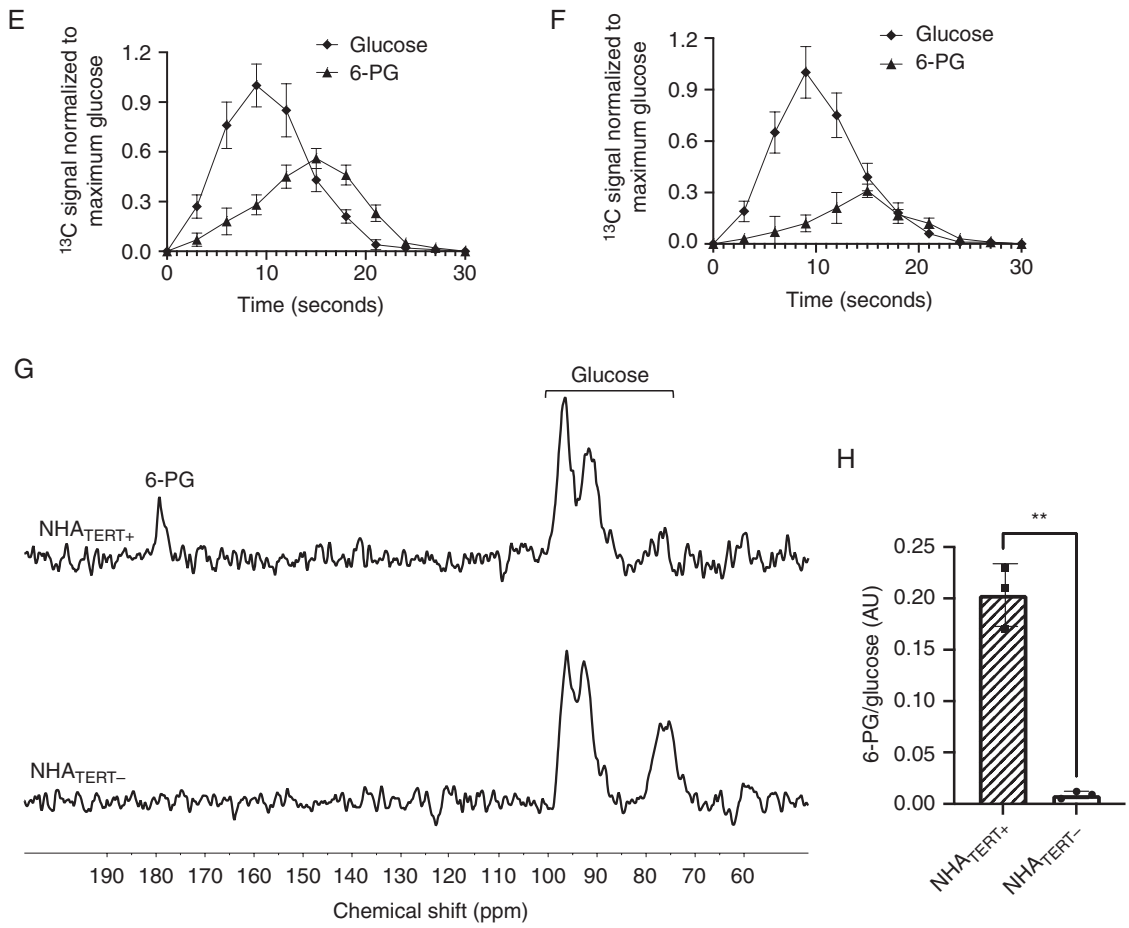

Fig. 3 Continued

we silenced TERT expression in a doxycycline-inducible manner in rats bearing orthotopic NHA$_{TERT+}$ tumors once tumors reached a volume of ~50 mm.[3] TERT expression and telomerase activity were significantly reduced following doxycycline treatment without alterations in tumor volume (Supplementary Figure S5A–C), consistent with previous studies pointing to a lag period before cell death occurs due to TERT knockdown.[38] Importantly, doxycycline-induced TERT silencing abrogated 6-PG production *in vivo* (Figure 3G, H). There was no difference in the SNR of hyperpolarized glucose (Supplementary Figure S5D), indicating that loss of 6-PG production did not result from differences in glucose delivery.

Finally, to assess the spatial distribution of hyperpolarized [U-^{13}C, U-^{2}H]-glucose metabolism, we performed 2D EPSI on rats bearing orthotopic NHA$_{TERT+}$ or SF10417 tumors. Metabolic heatmaps generated by overlaying ^{13}C data acquired at 15 seconds post-injection of hyperpolarized [U-^{13}C, U-^{2}H]-glucose (corresponding to the time-point of maximum 6-PG in slab studies; see Figure 3E, F) on the anatomical MRI indicated localization of 6-PG to the tumor while glucose was distributed throughout the brain (Figure 4A, B). Importantly, consistent with the slab studies, the 6-PG/glucose ratio differentiated tumor from contralateral normal brain while there was no difference in the SNR of hyperpolarized [U-^{13}C, U-^{2}H]-glucose (Figure 4C–F). Collectively, these results suggest that 6-PG production from hyperpolarized [U-^{13}C, U-^{2}H]-glucose is a metabolic imaging biomarker of TERT expression *in vivo*, including in clinically relevant patient-derived LGOG models.

TERT Acts via SIRT2 to Modulate GLUT1 and G6PDH Expression in LGOGs

To identify the molecular mechanisms by which TERT modulates PPP flux in LGOGs, we interrogated enzymes and transporters involved in glucose metabolism upstream of 6-PG (see schematic in Figure 1D). In line with PPP flux (see Figure 1B), G6PDH expression (Supplementary Figure S6A) and activity (Figure 5A) were downregulated by doxycycline-induced TERT silencing in the NHA$_{TERT+}$ model. Expression of the glucose transporter GLUT1 (Figure 5B and Supplementary Figure S6B) and [2-^{13}C]-glucose uptake (Supplementary Figure S6C) were also reduced in NHA$_{TERT-}$ cells. There was no alteration

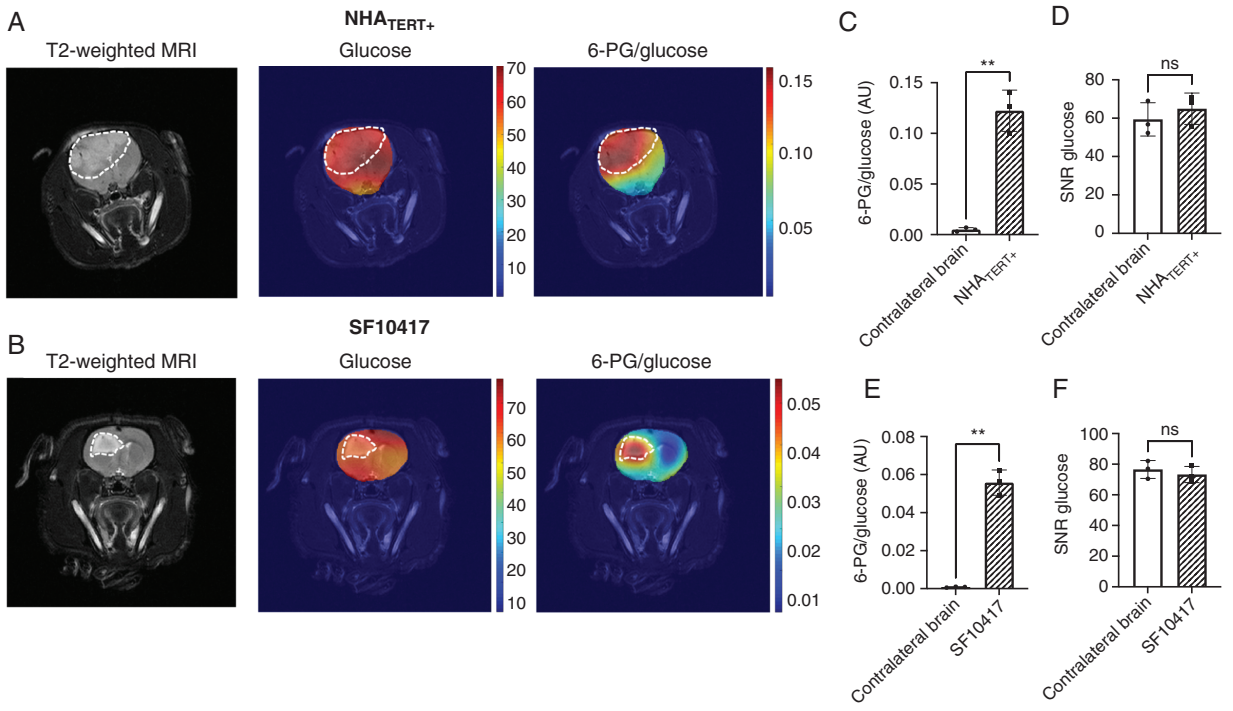

Fig. 4 Hyperpolarized [U-^{13}C, U-^{2}H]-glucose noninvasively monitors tumor burden in LGOGs *in vivo*. (A) Left panel: Representative T2-weighted MRI from an NHA$_{TERT+}$ tumor-bearing rat with the tumor contoured in white. Middle panel: Metabolic heatmap of hyperpolarized [U-^{13}C, U-^{2}H]-glucose distribution overlaid over the corresponding MRI; Right panel: Metabolic heatmap of [1-^{13}C]-6-PG distribution. (B) Left panel: Representative T2-weighted MRI from a rat bearing an orthotopic SF10417 tumor. The tumor is outlined in white. Middle panel: Metabolic heatmap of hyperpolarized [U-^{13}C, U-^{2}H]-glucose distribution overlaid over the corresponding MRI; Right panel: Metabolic heatmap of hyperpolarized 6-PG production. 6-PG/glucose ratio (C) and the SNR of hyperpolarized [U-^{13}C, U-^{2}H]-glucose (D) in rats bearing orthotopic NHA$_{TERT+}$ tumors. 6-PG/glucose ratio (E) and the SNR of hyperpolarized [U-^{13}C, U-^{2}H]-glucose (F) in SF10417 tumor-bearing rats. Abbreviations: LGOG, low-grade oligodendrogliomas; SNR, signal-to-noise ratio.

in hexokinase activity (Supplementary Figure S6D). TERT silencing also downregulated GLUT1 and G6PDH in the patient-derived SF10417 model (Supplementary Figure S6E, F). Importantly, GLUT1 and G6PDH were downregulated in *ex vivo* tumor tissues resected from rats bearing NHA$_{TERT-}$ tumors relative to NHA$_{TERT+}$ (Supplementary Figure S6G, H).

To assess the role of GLUT1 and G6PDH in TERT-linked upregulation of PPP flux, we examined the effect of silencing GLUT1 or G6PDH in BT54 neurospheres. GLUT1 silencing (Supplementary Figure S7A) significantly reduced [2-^{13}C]-glucose uptake (Supplementary Figure S7B). Although PPP fractional flux was unaltered (both PPP-derived [4-^{13}C]-glutamate and glycolysis-derived [5-^{13}C]-glutamate were reduced; Supplementary Figure S7C–E), 6-PG production from hyperpolarized [U-^{13}C, U-^{2}H]-glucose was significantly reduced in BT54 GLUT1– neurospheres (Figure 5C). These results suggest that TERT-mediated increase in GLUT1 leads to higher glucose uptake, which, in turn, leads to higher availability of glucose for PPP flux. Silencing G6PDH in BT54 neurospheres (Supplementary Figure S7F) also reduced 6-PG production from hyperpolarized [U-^{13}C, U-^{2}H]-glucose (Figure 5D), in line with results from the NHA$_{TERT+}$ model (Figure 2D).

The sirtuin SIRT2 has been shown to activate G6PDH and enhance NADPH production in mammalian cells.[39,40] SIRT2 expression was significantly reduced by doxycycline-mediated TERT silencing in the NHA$_{TERT+}$ model (Figure 5E). TERT silencing also downregulated SIRT2 expression in BT54 neurospheres (Figure 5F). Importantly, silencing SIRT2 in NHA$_{TERT+}$ cells (Supplementary Figure S8A) downregulated PPP flux, GLUT1, and G6PDH (Figure 5G–I). Conversely, SIRT2 overexpression in NHA$_{TERT-}$ cells (Supplementary Figure S8B) rescued the reduction in PPP flux, GLUT1, and G6PDH caused by TERT silencing (Figure 5J–L). Collectively, these results mechanistically link TERT to SIRT2, which, in turn, upregulates GLUT1 and G6PDH, resulting in higher glucose uptake and flux via the PPP.

TERT Expression Is Associated With Metabolic Reprogramming in LGOG Patient Biopsies

To evaluate the clinical relevance of our metabolic biomarkers, we examined biopsies from LGOG patients and compared them to non-neoplastic gliosis biopsies and biopsies from low-grade astrocytoma tumors that do not express TERT.[9,10] In line with the results from preclinical models, TERT expression and telomerase activity in LGOG

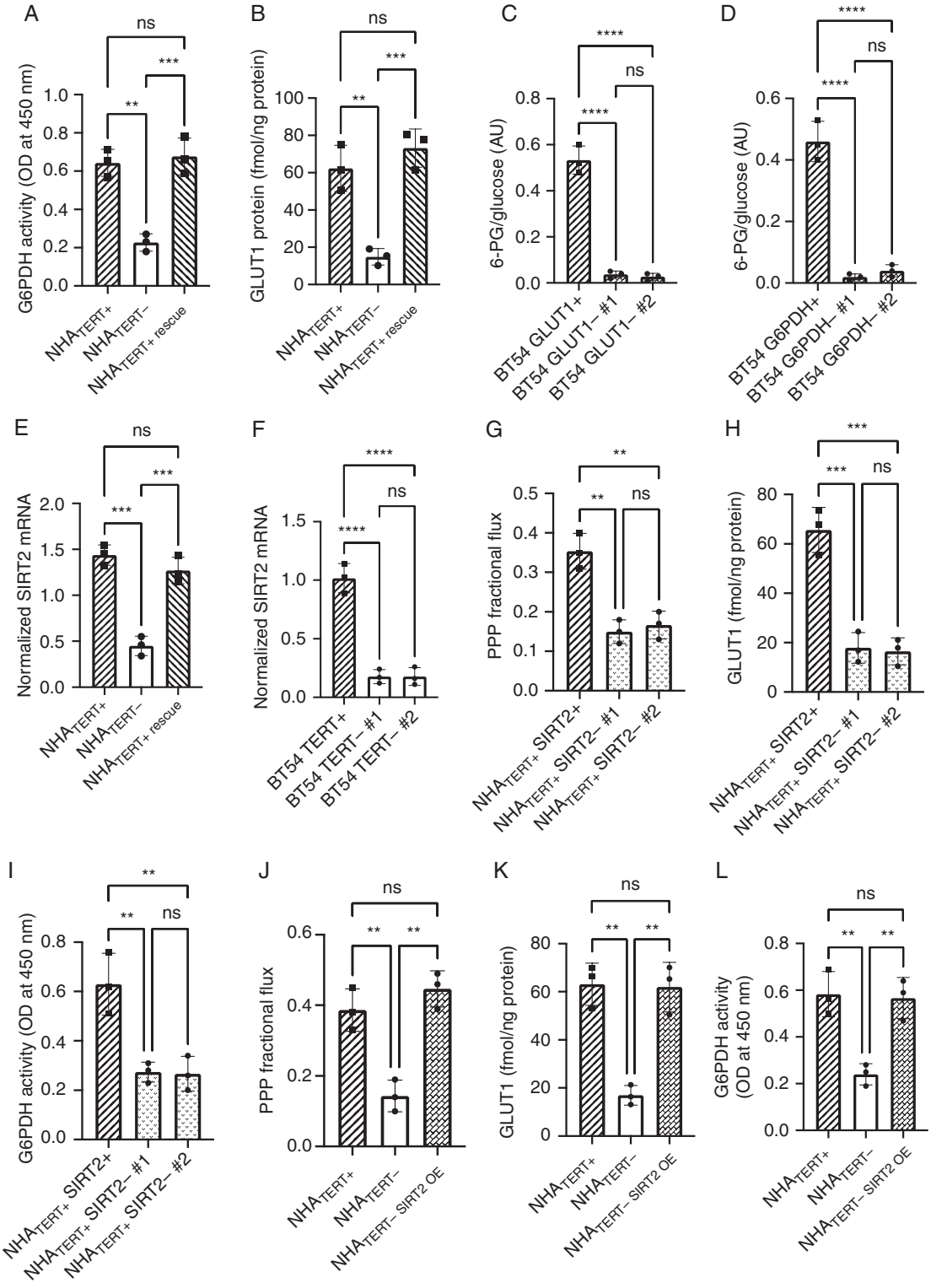

Fig. 5 TERT mechanistically modulates glucose metabolism in LGOGs. G6PDH activity (A) and GLUT1 protein (B) in NHA_{TERT+}, NHA_{TERT-}, and $NHA_{TERT+\ rescue}$ cells. Effect of GLUT1 (C) or G6PDH (D) silencing on 6-PG production from hyperpolarized glucose in BT54 neurospheres. (E) SIRT2 expression in NHA_{TERT+}, NHA_{TERT-}, and $NHA_{TERT+\ rescue}$ cells. (F) Effect of TERT silencing on SIRT2 expression in BT54 neurospheres. Effect of SIRT2 silencing on PPP flux (G), GLUT1 protein (H), and G6PDH activity (I) in NHA_{TERT+} cells. Effect of SIRT2 overexpression on PPP flux (J), GLUT1 protein (K), and G6PDH activity (L) in NHA_{TERT-} cells ($NHA_{TERT-SIRT2\ OE}$). Abbreviations: LGOG, low-grade oligodendrogliomas; PPP, pentose phosphate pathway; TERT, telomerase reverse transcriptase.

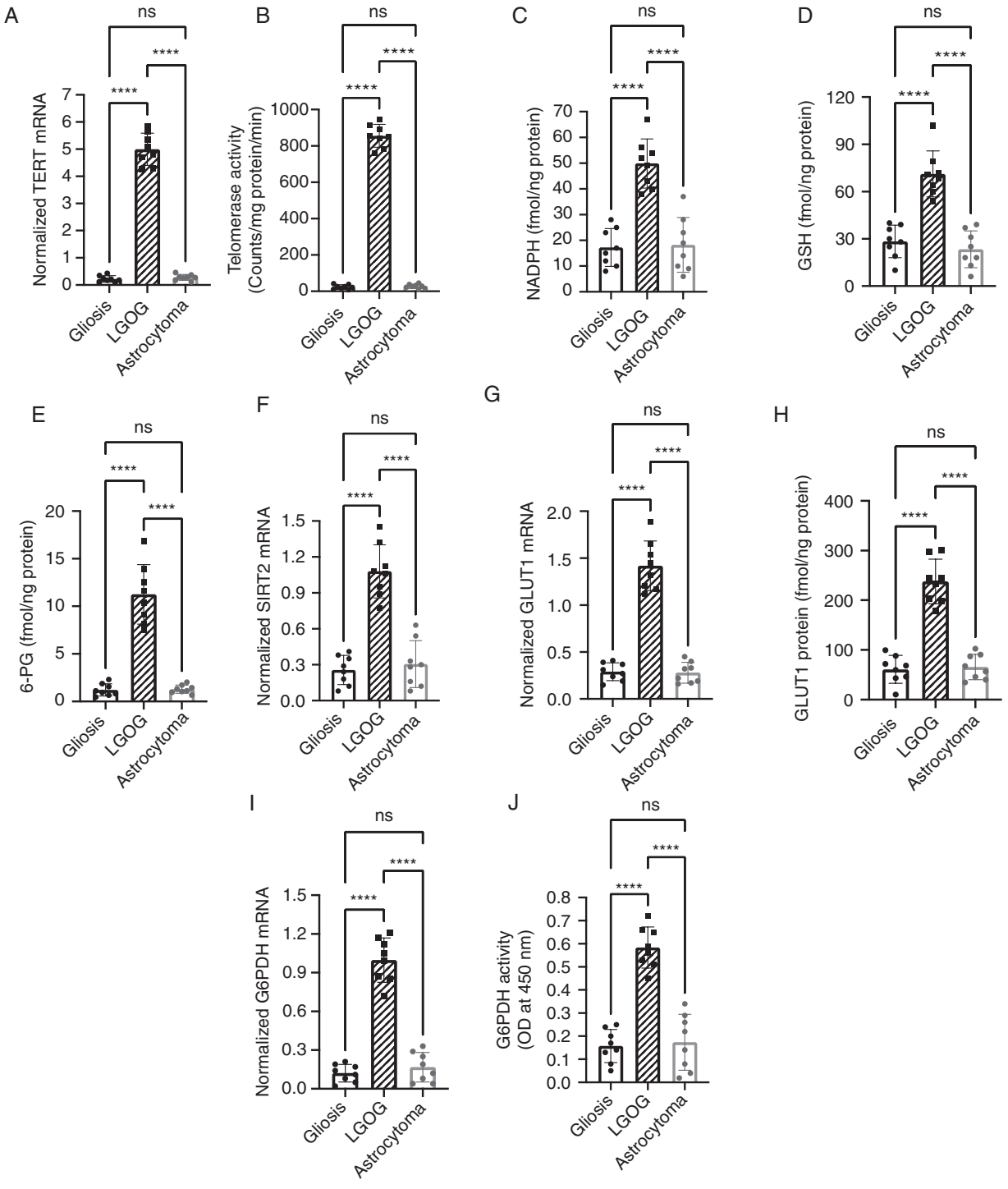

Fig. 6 TERT expression is linked to glucose metabolism in LGOG biopsies. TERT mRNA (A), telomerase activity (B), NADPH (C), GSH (D), 6-PG (E), SIRT2 mRNA (F), GLUT1 mRNA (G), GLUT1 protein (H), G6PDH mRNA (I), and G6PDH activity (J) in LGOG, gliosis, and astrocytoma biopsies. Abbreviations: GSH, glutathione; LGOG, low-grade oligodendrogliomas; TERT, telomerase reverse transcriptase.

biopsies (Figure 6A, B) were associated with elevated NADPH, GSH, 6-PG, SIRT2, GLUT1, and G6PDH relative to gliosis and astrocytoma (Figure 6C–J). These results link TERT to glucose metabolism in patient samples and point to the potential clinical utility of hyperpolarized glucose for assessing TERT status.

Discussion

TERT is indispensable for tumor proliferation, including in LGOGs.[1,2] Using NHAs that have been engineered to silence TERT in a doxycycline-inducible manner as well

as patient-derived LGOG models, we show that TERT upregulates glucose flux via the PPP and elevates antioxidant capacity. Importantly, we show that hyperpolarized [U-^{13}C, U-^{2}H]-glucose flux to 6-PG via the PPP can be used for noninvasive imaging of TERT expression in preclinical LGOG models *in vivo*.

Although we cannot rule out the possibility that glucose metabolism is modulated by other molecular pathways, our results point to a mechanistic association between TERT and the PPP in LGOGs. TERT silencing downregulates PPP flux, NADPH, and GSH in the NHA_{TERT+} and patient-derived LGOG models. Mechanistically, TERT acts by increasing GLUT1-mediated glucose uptake and upregulating G6PDH, the rate-limiting enzyme for 6-PG and NADPH synthesis. Importantly, the ability of SIRT2 overexpression to restore PPP flux, GLUT1, and G6PDH in NHA_{TERT-} cells and, conversely, the reduction in PPP flux, GLUT1, and G6PDH in NHA_{TERT+} cells in which SIRT2 is silenced, identify SIRT2 as a novel mediator of TERT-induced alterations in glucose metabolism.

Studies have used positron emission tomography (PET) or optical imaging for TERT detection.[41,42] However, the radioactive nature of PET limits longitudinal imaging due to concerns of radiation exposure while the restricted depth penetration of optical imaging limits application to gliomas. Recent studies have also used MRI combined with radiomics or ^{1}H-MRS to assess TERT status in LGOGs.[43,44] Our study identifies a complementary hyperpolarized ^{13}C-glucose-based method of imaging TERT status. 6-PG production from hyperpolarized [U-^{13}C, U-^{2}H]-glucose is consistently associated with TERT expression in LGOG cells and orthotopic tumors *in vivo*. In contrast, NHA_{ALT} cells and tumors that do not express TERT and, instead, use the ALT pathway for telomere maintenance,[22,23] produce lactate from hyperpolarized [U-^{13}C, U-^{2}H]-glucose, further confirming the utility of 6-PG production as a biomarker of TERT in LGOGs. Importantly, our results are significant in light of the limited utility of ^{18}F-fluorodeoxyglucose-positron emission tomography (FDG-PET) for glioma imaging, which stems from high glucose uptake in the normal brain.[45] The ability of 6-PG production to demarcate tumor from contralateral brain in our EPSI studies indicates that monitoring hyperpolarized ^{13}C-glucose metabolism to 6-PG, as opposed to monitoring glucose uptake by FDG-PET, can be useful for imaging glioma burden *in vivo*.

As an endogenous nutrient that readily crosses the blood-brain barrier[46] and is non-toxic at the doses in our study, hyperpolarized [U-^{13}C, U-^{2}H]-glucose has potential for clinical translation. The main limitation is the short T1 (~14 seconds at 3T). However, 6-PG has a relatively longer T1 (~32 seconds at 3T),[47] suggesting that clinically useful information can still be derived from the use of hyperpolarized [U-^{13}C, U-^{2}H]-glucose. A recent study[48] also achieved ~70% polarization for hyperpolarized [U-^{13}C, U-^{2}H]-glucose (as opposed to ~24% in our study), a method that could significantly improve the SNR. The use of singly labeled [2-^{13}C, U-^{2}H]-glucose[36] could also increase SNR since the resulting 6-PG peak would be a singlet.

Although some TERT inhibitors have encountered toxicity issues in clinical trials due to stem cell inhibition,[3] next-generation TERT inhibitors such as 6-thio-2′-deoxyguanosine have been successful in preclinical studies and are now in clinical trials.[49] Our studies show that 6-thio-2′-deoxyguanosine inhibits 6-PG production from hyperpolarized [U-^{13}C, U-^{2}H]-glucose in the patient-derived SF10417 model. Importantly, doxycycline-induced TERT silencing *in vivo* abrogates 6-PG production in the NHA_{TERT+} model. These results point to the potential utility of hyperpolarized [U-^{13}C, U-^{2}H]-glucose in monitoring response to TERT inhibitors and, thereby, enabling their clinical translation.

Glioma patient management is heavily dependent on MRI. However, distinguishing tumor from lesions such as gliosis and edema can be difficult using MRI. Importantly, MRI-based treatment response assessment is complicated by the occurrence of pseudoprogression, ie, treatment-related effects such as necrosis and inflammation that mimic tumor recurrence.[50] Our studies showing that TERT expression is associated with alterations in glucose metabolism in LGOG patient biopsies relative to gliosis point to the potential utility of metabolic imaging of TERT status for differentiating tumor from gliosis. Further studies *in vivo* are needed to fully determine the utility of hyperpolarized glucose in differentiating tumors from gliosis, pseudoprogression, or pseudoresponse.

In summary, our study mechanistically links TERT expression to elevated PPP flux and identifies hyperpolarized [U-^{13}C, U-^{2}H]-glucose as a potential metabolic imaging probe of TERT in LGOGs. By enabling noninvasive assessment of a hallmark of tumor immortality, our study has the potential to improve longitudinal tumor imaging and treatment response monitoring in LGOG patients.

Supplementary Material

Supplementary material is available at *Neuro-Oncology* online.

Keywords

gliomas | glucose metabolism | hyperpolarized ^{13}C | magnetic resonance spectroscopy | telomerase

Funding

This work was supported by: National Institutes of Health (R01CA239288 to P.V., S.M.R.; UCSF SPORE Career Enhancement Award P50CA97257 to P.V.; P01CA118816 to S.M.R., R01NS105087 to R.O.P., P41EB013598 Center grant), Department of Defense (W81XWH201055315 to P.V.), American Cancer Society (131715-RSG-18-005-01-CCE to P.E.Z.L.), NICO.

Conflict of interest statement. The authors have no conflicting interests to disclose.

Authorship statement. P.V. and S.M.R. conceptualized the research; P.V. designed the experiments; P.V., G.B., C.T., and V.A. performed experiments; A.M.G. assisted with cell and *in vivo* studies; P.E.Z.L. contributed to the design of imaging studies; H.A.L., J.F.C., and R.O.P. provided cell lines; P.V. wrote the manuscript; G.B. commented on the manuscript; P.V., S.M.R., and R.O.P. secured funding.

References

1. Hanahan D, Weinberg RA. Hallmarks of cancer: the next generation. *Cell.* 2011;144(5):646–674.
2. Shay JW, Wright WE. Telomeres and telomerase: three decades of progress. *Nat Rev Genet.* 2019;20(5):299–309.
3. Bell RJ, Rube HT, Xavier-Magalhães A, et al. Understanding TERT promoter mutations: a common path to immortality. *Mol Cancer Res.* 2016;14(4):315–323.
4. Akıncılar SC, Khattar E, Boon PL, Unal B, Fullwood MJ, Tergaonkar V. Long-range chromatin interactions drive mutant TERT promoter activation. *Cancer Discov.* 2016;6(11):1276–1291.
5. Mancini A, Xavier-Magalhaes A, Woods WS, et al. Disruption of the beta1L Isoform of GABP reverses glioblastoma replicative immortality in a TERT promoter mutation-dependent manner. *Cancer Cell.* 2018;34(3):513–528.e8.
6. Korber V, Yang J, Barah P, et al. Evolutionary trajectories of IDH^{WT} glioblastomas reveal a common path of early tumorigenesis instigated years ahead of initial diagnosis. *Cancer Cell.* 2019;35(4):692–704.e12.
7. Louis DN, Perry A, Reifenberger G, et al. The 2016 World Health Organization classification of tumors of the central nervous system: a summary. *Acta Neuropathol.* 2016;131(6):803–820.
8. Eckel-Passow JE, Lachance DH, Molinaro AM, et al. Glioma groups based on 1p/19q, IDH, and TERT promoter mutations in tumors. *N Engl J Med.* 2015;372(26):2499–2508.
9. Dilley RL, Greenberg RA. ALTernative telomere maintenance and cancer. *Trends Cancer.* 2015;1(2):145–156.
10. Ferreira MSV, Sørensen MD, Pusch S, et al. Alternative lengthening of telomeres is the major telomere maintenance mechanism in astrocytoma with isocitrate dehydrogenase 1 mutation. *J Neurooncol.* 2020;147(1):1–14.
11. Pekmezci M, Rice T, Molinaro AM, et al. Adult infiltrating gliomas with WHO 2016 integrated diagnosis: additional prognostic roles of ATRX and TERT. *Acta Neuropathol.* 2017;133(6):1001–1016.
12. Li Y, Tergaonkar V. Noncanonical functions of telomerase: implications in telomerase-targeted cancer therapies. *Cancer Res.* 2014;74(6):1639–1644.
13. Bagheri S, Nosrati M, Li S, et al. Genes and pathways downstream of telomerase in melanoma metastasis. *Proc Natl Acad Sci USA.* 2006;103(30):11306–11311.
14. Ahmad F, Dixit D, Sharma V, et al. Nrf2-driven TERT regulates pentose phosphate pathway in glioblastoma. *Cell Death Dis.* 2016;7:e2213.
15. Ahmad F, Patrick S, Sheikh T, et al. Telomerase reverse transcriptase (TERT) - enhancer of zeste homolog 2 (EZH2) network regulates lipid metabolism and DNA damage responses in glioblastoma. *J Neurochem.* 2017;143(6):671–683.
16. Ahmed S, Passos JF, Birket MJ, et al. Telomerase does not counteract telomere shortening but protects mitochondrial function under oxidative stress. *J Cell Sci.* 2008;121(Pt 7):1046–1053.
17. Indran IR, Hande MP, Pervaiz S. hTERT overexpression alleviates intracellular ROS production, improves mitochondrial function, and inhibits ROS-mediated apoptosis in cancer cells. *Cancer Res.* 2011;71(1):266–276.
18. Kurhanewicz J, Vigneron DB, Ardenkjaer-Larsen JH, et al. Hyperpolarized ^{13}C MRI: path to clinical translation in oncology. *Neoplasia.* 2019;21(1):1–16.
19. Viswanath P, Li Y, Ronen SM. C-13 Hyperpolarized MR spectroscopy for metabolic imaging of brain tumors. In: Pope WB, ed. *Glioma Imaging: Physiologic, Metabolic, and Molecular Approaches.* Cham: Springer International Publishing; 2020:191–209.
20. Park I, Larson PEZ, Gordon JW, et al. Development of methods and feasibility of using hyperpolarized carbon-13 imaging data for evaluating brain metabolism in patient studies. *Magn Reson Med.* 2018;80(3):864–873.
21. Ohba S, Mukherjee J, Johannessen TC, et al. Mutant IDH1 expression drives TERT promoter reactivation as part of the cellular transformation process. *Cancer Res.* 2016;76(22):6680–6689.
22. Mukherjee J, Johannessen TC, Ohba S, et al. Mutant IDH1 cooperates with ATRX loss to drive the alternative lengthening of telomere phenotype in glioma. *Cancer Res.* 2018;78(11):2966–2977.
23. Viswanath P, Batsios G, Mukherjee J, et al. Non-invasive assessment of telomere maintenance mechanisms in brain tumors. *Nat Commun.* 2021;12(1):92.
24. Jones LE, Hilz S, Grimmer MR, et al. Patient-derived cells from recurrent tumors that model the evolution of IDH-mutant glioma. *Neurooncol Adv.* 2020;2(1):vdaa088.
25. Kelly JJ, Blough MD, Stechishin OD, et al. Oligodendroglioma cell lines containing t(1;19)(q10;p10). *Neuro Oncol.* 2010;12(7):745–755.
26. Viswanath P, Radoul M, Izquierdo-Garcia JL, et al. Mutant IDH1 gliomas downregulate phosphocholine and phosphoethanolamine synthesis in a 2-hydroxyglutarate-dependent manner. *Cancer Metab.* 2018;6:3.
27. Viswanath P, Radoul M, Izquierdo-Garcia JL, et al. 2-Hydroxyglutarate-mediated autophagy of the endoplasmic reticulum leads to an unusual downregulation of phospholipid biosynthesis in mutant IDH1 gliomas. *Cancer Res.* 2018;78(9):2290–2304.
28. Rodrigues TB, Serrao EM, Kennedy BW, Hu DE, Kettunen MI, Brindle KM. Magnetic resonance imaging of tumor glycolysis using hyperpolarized ^{13}C-labeled glucose. *Nat Med.* 2014;20(1):93–97.
29. Cawthorne C, Swindell R, Stratford IJ, Dive C, Welman A. Comparison of doxycycline delivery methods for Tet-inducible gene expression in a subcutaneous xenograft model. *J Biomol Tech.* 2007;18(2):120–123.
30. Larson PE, Kerr AB, Chen AP, et al. Multiband excitation pulses for hyperpolarized ^{13}C dynamic chemical-shift imaging. *J Magn Reson.* 2008;194(1):121–127.
31. Brekke EM, Walls AB, Schousboe A, Waagepetersen HS, Sonnewald U. Quantitative importance of the pentose phosphate pathway determined by incorporation of ^{13}C from [2-^{13}C]- and [3-^{13}C] glucose into TCA cycle intermediates and neurotransmitter amino acids in functionally intact neurons. *J Cereb Blood Flow Metab.* 2012;32(9):1788–1799.
32. Stincone A, Prigione A, Cramer T, et al. The return of metabolism: biochemistry and physiology of the pentose phosphate pathway. *Biol Rev Camb Philos Soc.* 2015;90(3):927–963.
33. Christensen CE, Karlsson M, Winther JR, Jensen PR, Lerche MH. Non-invasive in-cell determination of free cytosolic [NAD^+]/[NADH] ratios using hyperpolarized glucose show large variations in metabolic phenotypes. *J Biol Chem.* 2014;289(4):2344–2352.
34. Harris T, Degani H, Frydman L. Hyperpolarized ^{13}C NMR studies of glucose metabolism in living breast cancer cell cultures. *NMR Biomed.* 2013;26(12):1831–1843.

35. Timm KN, Hartl J, Keller MA, et al. Hyperpolarized [U-^{2}H, U-^{13}C] Glucose reports on glycolytic and pentose phosphate pathway activity in EL4 tumors and glycolytic activity in yeast cells. *Magn Reson Med.* 2015;74(6):1543–1547.
36. Mishkovsky M, Anderson B, Karlsson M, et al. Measuring glucose cerebral metabolism in the healthy mouse using hyperpolarized ^{13}C magnetic resonance. *Sci Rep.* 2017;7(1):11719.
37. Mender I, Gryaznov S, Dikmen ZG, Wright WE, Shay JW. Induction of telomere dysfunction mediated by the telomerase substrate precursor 6-thio-2′-deoxyguanosine. *Cancer Discov.* 2015;5(1):82–95.
38. Patel PL, Suram A, Mirani N, Bischof O, Herbig U. Derepression of hTERT gene expression promotes escape from oncogene-induced cellular senescence. *Proc Natl Acad Sci USA.* 2016;113(34):E5024–E5033.
39. Xu SN, Wang TS, Li X, Wang YP. SIRT2 activates G6PD to enhance NADPH production and promote leukaemia cell proliferation. *Sci Rep.* 2016;6:32734.
40. Wang YP, Zhou LS, Zhao YZ, et al. Regulation of G6PD acetylation by SIRT2 and KAT9 modulates NADPH homeostasis and cell survival during oxidative stress. *EMBO J.* 2014;33(12):1304–1320.
41. Jung KO, Youn H, Kim SH, Kim YH, Kang KW, Chung JK. A new fluorescence/PET probe for targeting intracellular human telomerase reverse transcriptase (hTERT) using Tat peptide-conjugated IgM. *Biochem Biophys Res Commun.* 2016;477(3):483–489.
42. Liu M, Wang RF, Zhang CL, et al. Noninvasive imaging of human telomerase reverse transcriptase (hTERT) messenger RNA with ^{99m}Tc-radiolabeled antisense probes in malignant tumors. *J Nucl Med.* 2007;48(12):2028–2036.
43. Park YW, Ahn SS, Park CJ, et al. Diffusion and perfusion MRI may predict EGFR amplification and the TERT promoter mutation status of IDH-wildtype lower-grade gliomas. *Eur Radiol.* 2020;30(12):6475–6484.
44. Fukuma R, Yanagisawa T, Kinoshita M, et al. Prediction of IDH and TERT promoter mutations in low-grade glioma from magnetic resonance images using a convolutional neural network. *Sci Rep.* 2019;9(1):20311.
45. la Fougère C, Suchorska B, Bartenstein P, Kreth FW, Tonn JC. Molecular imaging of gliomas with PET: opportunities and limitations. *Neuro Oncol.* 2011;13(8):806–819.
46. Hertz MM, Paulson OB. Glucose transfer across the blood–brain barrier. *Adv Metab Disord.* 1983;10:177–192.
47. Moreno KX, Harrison CE, Merritt ME, Kovacs Z, Malloy CR, Sherry AD. Hyperpolarized δ-[1-^{13}C]gluconolactone as a probe of the pentose phosphate pathway. *NMR Biomed.* 2017;30(6):e3713.
48. Capozzi A, Patel S, Wenckebach WT, Karlsson M, Lerche MH, Ardenkjær-Larsen JH. Gadolinium effect at high-magnetic-field DNP: 70% ^{13}C polarization of [U-^{13}C] glucose using trityl. *J Phys Chem Lett.* 2019;10(12):3420–3425.
49. Sengupta S, Sobo M, Lee K, et al. Induced telomere damage to treat telomerase expressing therapy-resistant pediatric brain tumors. *Mol Cancer Ther.* 2018;17(7):1504–1514.
50. Villanueva-Meyer JE, Mabray MC, Cha S. Current clinical brain tumor imaging. *Neurosurgery.* 2017;81(3):397–415.